

# Universal Transformation of One-Class Classifiers for Unsupervised Anomaly Detection

Declan McIntosh  
 University of Victoria  
 B.C., Canada  
 declanmcintosh@uvic.ca

Alexandra Branzan Albu  
 University of Victoria  
 B.C., Canada  
 aalbu@uvic.ca

## Abstract

*Detecting anomalies in images and video is an essential task for multiple real-world problems, including industrial inspection, computer-assisted diagnosis, and environmental monitoring. Anomaly detection is typically formulated as a one-class classification problem, where the training data consists solely of nominal values, leaving methods built on this assumption susceptible to training label noise. We present a dataset folding method that transforms an arbitrary one-class classifier-based anomaly detector into a fully unsupervised method. This is achieved by making a set of key weak assumptions: that anomalies are uncommon in the training dataset and generally heterogeneous. These assumptions enable us to utilize multiple independently trained instances of a one-class classifier to filter the training dataset for anomalies. This transformation requires no modifications to the underlying anomaly detector; the only changes are algorithmically selected data subsets used for training. We demonstrate that our method can transform a wide variety of one-class classifier anomaly detectors for both images and videos into unsupervised ones. Our method creates the first unsupervised logical anomaly detectors by transforming existing methods. We also demonstrate that our method achieves state-of-the-art performance for unsupervised anomaly detection on the MVTec AD, ViSA, and MVTec Loco AD datasets. As improvements to one-class classifiers are made, our method directly transfers those improvements to the unsupervised domain, linking the domains. Code: [Link Held For Review](#).*

## 1. Introduction

Anomaly detection broadly seeks to identify uncommon or novel structures in data. Anomaly detection and localization for images and video is a field of key interest for many application domains, including industrial inspection, medical imaging, video surveillance, biodiversity assessment,

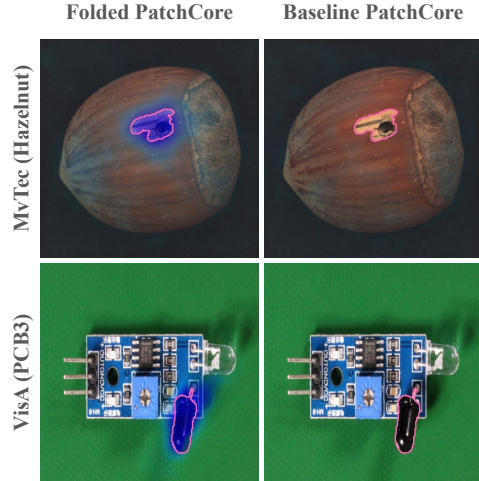


Figure 1. Comparison of prediction on training corruptions of PatchCore with and without folding. Folding was done with 3 votes and 4 folds. Pink outlines are the anomaly ground truth, and regions of increasingly darker blue are predicted anomalies.

and environmental monitoring [4, 7]. However, industrial inspection remains the most common application [3, 39]. In these contexts, anomalies can be defects, pathologies, or novel species behaviors; the automatic detection of each of these is highly relevant for its respective field [3, 11, 39].

Modern One-Class Classification (OCC)-based anomaly detection methods have demonstrated excellent performance in image anomaly detection, using a plethora of diverse strategies [4, 29]. Further methods have been developed to address diverse application-specific considerations, including logical anomaly detection, low-latency anomaly detection, RGB-D anomaly detection, and multi-view anomaly detection [3, 5, 39]. These methods perform very well on their respective benchmarks but still universally use the OCC problem formulation, assuming the training dataset consists only of the nominal class [3, 41]. So, while these methods can detect more diverse types of anomalies

or detect anomalies much faster, they still require a manually curated nominal dataset; otherwise, they will learn the present anomalies at training as nominal [26, 41]. In Figure 1, PatchCore, an OCC method, is shown missing clearly apparent anomalies because they were present during training. This is especially troubling for applications where nominal data may not be known a priori, such as in biodiversity assessment or environmental monitoring [6, 25]. Furthermore, in real-world deployments, even with manually curated datasets, label noise is inevitably present [23].

Several fully unsupervised anomaly detection methods have been developed to address this, offering high tolerance to training anomalies and thereby removing the need for OCC assumptions and broadening the real-world applicability of anomaly detection methods [17, 26]. However, these methods perform worse than existing OCC methods when anomalies are absent during training, resulting in a trade-off between anomaly detection performance and noise tolerance [27, 41]. Furthermore, these methods lack the diversity of existing OCC methods, as they independently converged on patch-based approaches [26, 41]. Due to this convergence adapting existing fully unsupervised anomaly detection methods to more diverse applications, such as logical anomalies, would require fundamental changes to their approaches [17, 26, 41].

To solve current limitations in unsupervised anomaly detection methods, we propose a method of folding datasets to transform any existing OCC method to be applied on unsupervised data, which is described in Section 3. This is achieved using a small set of weak assumptions about the general anomaly detection problem, stated in Sections 3.1 & 3.2. In this paper, our proposed transformation is applied to a diverse set of OCC methods and anomaly detection tasks, including logical anomalies and video anomaly detection in Section 4.

#### Our work’s key contributions include:

- A method for adapting arbitrary existing and future OCC anomaly detection methods to operate fully unsupervised without modification, for both image and video.
- New state-of-the-art results in unsupervised anomaly detection on the MvTecAD, ViSA, and LOCO AD datasets using transformations of existing OCC methods.
- Presenting the first unsupervised logical anomaly detection method.

## 2. Related Works

### 2.1. One-Class Classifier Anomaly Detectors

The vast majority of image anomaly detection methods rely on a one-class classification assumption, where all training data is drawn from the nominal class [4, 7, 9]. This allows these methods to model the entire training dataset and test new data to assess its conformity with the model and detect

anomalies as outliers to this model [33]. There are two key parts to these methods in general: how they model the nominal training data, and how they measure conformity of new data to this model [9]. Since these components are so openly defined, a diverse literature of OCC methods exists [9].

Reconstruction methods aim to degrade images with synthetic anomalies, then reconstruct the original clean sample to model the nominal distribution by learning a mapping from corrupted images to their nominal counterparts [44, 47]. Then, at inference, they compare the unknown sample to its reconstruction, where significant differences are likely anomalies being mapped back to the learned nominal space [18, 19, 38]. These methods are very similar to self-supervised methods, which also corrupt nominal training images and then learn to classify between the synthetic corruptions and the nominal images [12, 50]. Even within methods that use synthetic corruptions, the best generation method remains an active research question [16, 50]. Similarly, some methods utilize the structure of training General Adversarial Networks to train both a model for generating convincing fake nominal images and a discriminator that distinguishes between real and synthetic images [20, 42]. Then, at test time, the discriminator from the GAN is used to predict images as nominal or anomalous [20].

Some methods extract features from training images, model them as multivariate Gaussians, and test new images against these distributions [32, 45]. Further, some methods use an autoencoder structure, where they learn a compact latent representation of the training nominal images [8, 43]. Then, at test time, they pass images through the autoencoder and check for regions of poor reconstruction, which indicate that anomalies are present since they were not well represented in the learned compact latent space [3, 8]. Still, other methods employ a student-teacher architecture, where a single teacher model is trained to generate features from a large set of diverse images [3, 48]. Then, the student learns to mimic the teacher’s outputs, but only on the nominal set of images [34]. At test time, the difference between the student and teacher network-generated features is used to discriminate anomalies as regions of significant differences between student and teacher outputs [34, 48]. Patch-based methods use pre-trained feature extractors to describe image patches, then compare the set of nominal patch features with the test image patch features to distinguish anomalies based on high distances from training nominal features [10, 33, 46].

We reviewed here just a subset of the most popular and effective OCC method types for anomaly detection and localization, excluding less common methods such as normalized flow-based methods, attention-based methods, and density estimation [13, 21, 36].

## 2.2. Unsupervised Anomaly Detectors

Notably, all methods designed for OCC described in Section 2.1 are not intended to tolerate anomalies corrupting the training dataset [27, 41]. This means that if corruption exists in the training dataset, the trained OCC method will incorporate that anomaly into its nominal model and will likely be blind to similar anomalies when deployed. To address this, several methods have been developed to operate unsupervised, with sufficient tolerance to anomalies that they do not require guarantees of purely nominal datasets [27, 41]. These methods, however, exhibit much less diversity in approach; specifically, they all operate as patch-based methods that use a memory bank of previously seen features to distinguish anomalies from nominal data [17, 26]. In fact, all of these methods leverage statistical relationships between nominal and anomalous patch features to either filter or downweight anomalies in the training data [17, 41].

InReaCh and Online-InReaCh work by building their nominal patch set from only symmetrically minimum-distance pairs of patches between images [26, 27]. This approach assumes that nominal patches are common across images and that they should be more homogeneous than anomalies across image realizations [26, 27]. SoftPatch operates by performing patch-level noise discrimination, predicting the outlier score for each patch based on the Local Outlier Factor calculated from a memory bank of all patches [41]. They then remove the top  $\tau$  percentage of patches based on their outlier scores. Finally, FUN-AD considers that the distribution of distances between nominal-nominal patch pairs is distinct from that of anomaly-anomaly and nominal-anomaly pairs [17]. Using this, they can iteratively reconstruct their memory bank of predicted nominal patches to generate a final nominal memory bank for comparisons at test time [17].

Our proposed approach, described in Section 3 addresses the apparent lack of diversity in unsupervised anomaly detection methods by adapting any existing or future OCC method to be highly tolerant to training anomaly corruptions.

## 3. Proposed Approach

Our method adapts an existing OCC method and applies it to unsupervised datasets for anomaly detection, where the training data may be corrupted with anomalies, thereby violating a necessary OCC assumption. This is done by leveraging key assumptions presented in Section 3.1, which directly motivate our corollary in Section 3.2. Following this, in Section 3.3, we present a dataset folding method based on this corollary. We also present a variant of our method for video anomaly detection in Section 3.4. An overview of the method is presented in Figure 2.

## 3.1. Assumptions

$$|A| \gg |N| \quad (1)$$

Where  $A$  is the set of all possible samples considered anomalous,  $N$  is the set of all possible samples considered nominal for a given task.

For Equation 1, we are assuming that the magnitude of the set of all possible samples that would be considered anomalous is much larger than the set of all possible nominal samples. This can be justified by noting that, for any nominal sample  $x_n$ , many possible transformations can corrupt it into a unique anomalous sample  $x_a$ . For a concrete example, given any nominal image of a specific screw, there is a large set of possible unique scratches or objects placed on the screw which would constitute anomalies. Further, we can consider the sets  $A$  and  $N$  to be subsets of  $I$  (the space of all possible samples). Since anomaly detection is a binary consideration, all samples from  $I$  must be uniquely in either set,  $I = A \cup N$  [7, 9, 15]. From this, the set of all possible nominal images is a tiny set relative to all possible images and therefore anomalies, which, for a given resolution of  $256 \times 256$  pixels, is approximately  $5 \times 10^7$ .

$$P(x_i \in N) \gg P(x_i \in A) | x_i \sim F \quad (2)$$

In Equation 2, we are assuming that the probability of independently sampling an anomaly from the underlying image distribution  $F$  is much lower than the probability of independently sampling a nominal image, which we take directly from the anomaly detection problem definition [7, 9, 15]. Notably, we also assume, in our formulation of Equation 2, that each sample from the image distribution  $F$  is independent. This assumption could conceivably be broken if, for instance, a manufacturing defect creates a consistent anomaly in all or most samples during the collection of training data. We will, however, demonstrate empirically in our testing that this independence assumption is weak and can be relaxed.

## 3.2. Corollary

$$0 \approx P(\{x_i, x_j\} \in A) P(|x_i - x_j| < \epsilon) | x_i, x_j \sim F \quad (3)$$

The Corollary in Equation 3 states that the probability of a pair of independent samples being both very similar to each other and both anomalous is near zero. This comes directly from our assumptions in Equation 1 and 2.

The first term of Equation 3 being a low value, comes directly from Equation 2, where if the samples are independent, then  $P(\{x_i, x_j\} \in A) = [P(x_i \in A)]^2$  when  $P(x_i \in A)$  is already assumed low from the anomaly detection problem definition.

For the second term of Equation 3, based on the assumption in Equation 1, the set of all possible anomalies is vast compared to the set of nominal images; therefore, the probability of two independently sampled anomalies being less

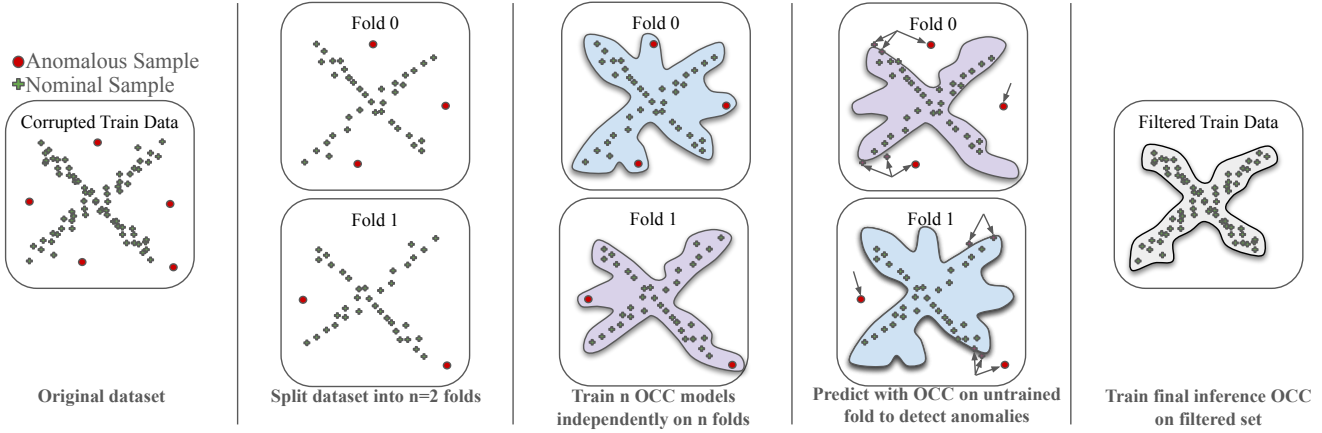


Figure 2. Folding process for removing anomalies from the training dataset for unsupervised anomaly detection with  $n=2$  folds. No assumptions are made about how the OCC anomaly detection model operates or the data type; our method only changes the subset of training data available to the OCC model at each step.

than  $\epsilon$  apart is low. In the context of our method,  $\epsilon$  represents the given OCC anomaly detector’s tolerance. We define tolerance as the minimum distance between two samples, such that if one were present during training, the other would be considered nominal by the trained OCC anomaly detector at inference.

The corollary is reinforced by the results of previous papers, where OCC methods perform almost indistinguishably from unsupervised anomaly detectors when the training corruptions are disjoint from the test set, as previously referred to as the ‘no-overlap’ case [41]. This is because the chance of two anomalies, separated into the training and testing sets, being less than  $\epsilon$  apart in the small, manually curated, and manually corrupted testing sets of used is very low [26, 41]. However, for longer-term deployment, the likelihood of anomalies sampled during inference being within  $\epsilon$  of any training anomaly corruptions increases significantly, necessitating the use of unsupervised anomaly detection methods to prevent false negatives.

The practical result of Equation 3 is that when a limited dataset of training samples is split, there is a low chance that any pairs of anomalies exist in separate subsets of that dataset which are also within a distance  $\epsilon$  of each other. Therefore, training on a subset with one or more anomalies will likely not cause the model to predict another anomaly as nominal when predicting on a separate independent subset. This result can be used to train a model on one subset of data to filter another subset, a process formalized in Section 3.3.

### 3.3. Folding Anomalies

Motivated by Equation 3, we develop a method that uses an unmodified arbitrary OCC anomaly-detection method to filter a dataset of potentially corrupted samples. We achieve this by first splitting the dataset randomly into  $n$

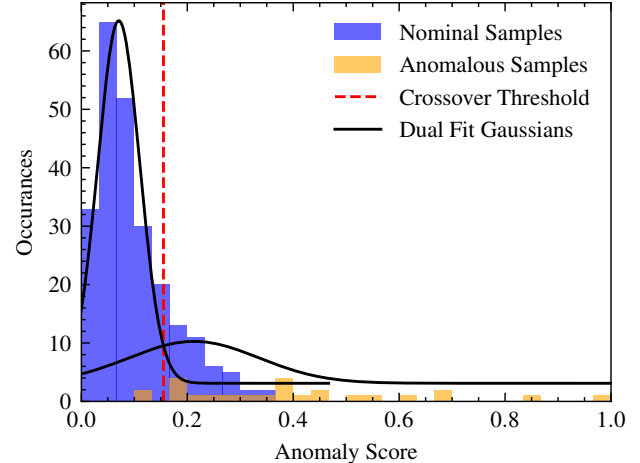


Figure 3. Example mixture of Gaussians over the predictions by PatchCore on the screw class of MvTecAD for a given fold. Nominal samples are shown in blue, and anomalous samples are shown in orange. The determined crossover threshold between the two fit Gaussians is shown as a red dotted line. The weight of each sample for the mixture of Gaussians was one minus its predicted anomaly value.

folds  $f_1, f_2, \dots, f_n$ , which are non-overlapping subsets of the original dataset, Line 2 of Algorithm 1. The union of these folds re-forms the original dataset. We then fit a separate instance of the anomaly detection model to each fold of the original dataset (Line 3). Each of these models predicts on all data, excluding the data on which it was trained (Line 4). Predictions are normalized to the range  $[0, 1]$ , where 1 represents an anomaly and 0 represents a nominal value (Line 5). For each of these sets of predictions excluding a fold, we

fit a mixture of two Gaussians (GMM) to the predictions (Line 6), which are biased towards nominal predictions, as shown in Figure 3 [31]. We bias the GMM towards nominal features by weighting each sample by one minus its predicted anomaly value, so highly anomalous outlier samples have a lesser effect on the Gaussian fit. This bias is chosen to ensure our filter has high precision, at the cost of lower recall of nominal images. Lower recall can be tolerated as OCC anomaly detectors are generally very data-efficient; therefore, the loss of nominal data is less detrimental [2]. The crossover point between these two Gaussian probability functions is taken as the filter threshold (Line 7). This is selected such that one distribution covers nominal samples and the other distribution covers anomalous samples, and nominal samples which are not well represented in the given fold. For each training sample, we record whether it was above or below the nominal threshold. If, in the majority of these per-fold predictions, a sample was predicted to be anomalous, it is removed from the candidate training dataset (Line 8). This entire process can be repeated multiple times with new random folds for  $k$  iterations, which we refer to as votes, such that the final training set is the average of the resulting datasets over multiple runs (Line 11). Once a final set of images is determined to be nominal, we train a final instance of the OCC on this filtered dataset (Line 12). We will denote any configuration of folds and votes in this paper as *OCC Method(# of votes/# of folds)*.

---

**Algorithm 1** *Folding Filtering*: Transformation of OCC method for Unsupervised Anomaly Detection

---

**Input:** Dataset  $D$ , OCC Anomaly Detection Method *TrainModel*, Number of folds  $n$ , number of votes  $K$   
**Output:** Trained OCC Anomaly Detector  $M_T$

- 1: **for**  $k \leftarrow 1$  to  $K$  **do**
- 2:    $\{D^{(i)}\}_{i=1}^n \leftarrow \text{RandomSplit}(D, n)$
- 3:    $\{M^{(i)}\}_{i=1}^n \leftarrow \{\text{TrainModel}(D^{(i)})\}_{i=1}^n$
- 4:    $P^{(i,j)}[x] \leftarrow \text{Predict}(M^{(j)}, D^{(i)}[x])$ ,  
 $\forall i \in [n], j \in [n] \setminus \{i\}, x \in [|D^{(i)}|]$
- 5:    $P \leftarrow \frac{P - \min(P)}{\max(P) - \min(P)}$
- 6:    $G_{1,2}^{(i)} \leftarrow \text{FitGMM}_{g=2}\left(\{P^{(i,j)}\}_{j \neq i},\right.$   
 $\left. \text{weight} = \{1 - P^{(i,j)}\}_{j \neq i}\right)$
- 7:    $T^{(i)} \leftarrow \text{Solve}(\text{PDF}(G_1^{(i)}) = \text{PDF}(G_2^{(i)}))$
- 8:    $D'^{(i)} \leftarrow D^{(i)} \setminus \left\{ D^{(i)}[x] \mid \#\{j \in [n] \setminus \{i\} \mid P^{(i,j)}[x] > T^{(i)}\} < \frac{n-1}{2} \right\}$
- 9:    $D^{(k)} \leftarrow \bigcup_{i=1}^n D'^{(i)}$
- 10: **end for**
- 11:  $D_f \leftarrow \text{MajorityVote}(\{D^{(k)}\}_{k=1}^K)$
- 12:  $M_T \leftarrow \text{TrainModel}(D_f)$
- 13: **return**  $M_T$

---

This method works as the likelihood that a specific anomaly is well represented in a majority of other folds is

expected to be very low. Therefore, by training our OCC anomaly detector on each fold, we are confident that despite the OCC method overfitting by design to its training data and learning any anomalies present in that fold to be nominal, these learned anomalies will not generalize to anomalies in other folds. A conceptual example of this can be seen in Figure 2, where, despite each of the two models fitting entirely to anomalies present in their training fold, the anomalies in the other fold were distinct and therefore not misclassified. This method requires an OCC to be run ( $\text{folds} \times \text{iterations} + 1$ ) times, which significantly increases offline training time. This proposed folding procedure makes no changes to the underlying OCC method; it only modifies the data available for each trained instance, ensuring that test-time inference remains identical. From this, any special considerations of the underlying OCC methods, such as the ability to detect logical anomalies or specific feature extractors for medical image domains, remain after the adaptation to unsupervised operation.

### 3.4. Modifications for Video Data

Generalizing our method for video requires changing the consideration of images to frames of video clips. To ensure independence between the folds, we split the entire video clips into separate folds. This is because each frame is highly dependent on its adjacent frames, but each video clip is independent of the others. So a single anomalous object across multiple frames in one video is not split onto multiple folds. We then train the OCC video anomaly detection method as usual on each fold and complete the entire folding anomalies procedure to determine anomalous frames to remove from the training set.

Once we have our filtered set of predicted anomalous frames, we perform a 2D morphological closing operation to reduce holes in the predicted anomalous frame regions, as we expect a frame flanked by anomalous frames also to be anomalous. Clips split by one or more regions of anomalous frames are split into separate clips in the final filtered training dataset. Finally, any clips shorter than 5 frames are discarded. Excluding these post-processing changes, all procedures for video dataset folding are the same as described in Algorithm 1.

## 4. Results

### 4.1. Testing Configuration

For all our experiments, we use the proposed methods at their prescribed resolutions, but we scale the predicted masks to 256x256 and center crop them to 224x224 for reporting P-AUROC and AUPRO values [3, 33]. This is done to accommodate the lowest-resolution predictions from any method, allowing for direct comparisons across all methods on all datasets [26, 33, 41]. We make minimal modifica-

Dataset [2, 49]	Metric	0% Corruptions				10% Corruptions			
		InReaCh [26]	SoftPatch [41]	FUN-AD [17]	Folded(3/4) PatchCore [33]	InReaCh [26]	SoftPatch [41]	FUN-AD [17]	Folded(3/4) PatchCore [33]
MvTecAD	I-AUROC	0.884	0.985	0.862	<b>0.992</b>	0.855	<b>0.984</b>	0.965	<b>0.984</b>
MvTecAD	P-AUROC	0.950	0.981	0.939	<b>0.982</b>	0.935	0.960	<b>0.975</b>	0.974
MvTecAD	AUPRO	0.825	0.929	0.748	<b>0.945</b>	0.805	0.903	0.888	<b>0.932</b>
ViSA	I-AUROC	0.777	0.915	0.810	<b>0.960</b>	0.730	0.893	0.909	<b>0.910</b>
ViSA	P-AUROC	0.959	0.984	0.906	<b>0.987</b>	0.944	0.887	0.929	<b>0.951</b>
ViSA	AUPRO	0.769	0.901	0.691	<b>0.939</b>	0.705	0.797	0.757	<b>0.879</b>
Average	I-AUROC	0.831	0.95	0.836	<b>0.976</b>	0.793	0.939	0.937	<b>0.947</b>

Table 1. Performance of unsupervised anomaly detectors on MvTecAD and ViSA datasets. Wrapped (3/4) PatchCore shows the best performance in anomaly detection (I-AUROC) on both datasets for corrupted datasets.

tions to specific methods to enable fully unsupervised use, such as removing hard-coded training lengths for specific target classes or the use of testing set performance to select optimal weight checkpoints at a specific epoch [17, 22]. Full details on all modifications to methods are available in the Supplemental Materials. All testing with a specific dataset and anomaly corruption proportion uses the same set of corruptions from the testing set. We conduct all our testing in the more challenging unsupervised overlapping setup, where anomaly corruptions observed during training are also present during testing [3, 17]. This contrasts with the non-overlapping task, where training anomalies are absent during testing.

## 4.2. Results on Image Anomaly Detection

We present results of our method, which extends unmodified PatchCore to enable unsupervised operation, achieving SOTA results among unsupervised methods on both uncorrupted and corrupted MvTecAD and ViSA, as shown in Table 1. We obtain results very similar to SoftPatch’s on the MvTecAD dataset, as expected, since SoftPatch is a modification of PatchCore designed to extend it to unsupervised anomaly detection [33, 41]. However, unlike existing baselines, we did not need to design our underlying anomaly detection method’s architecture to tolerate anomalies during training [17, 26, 41]. This enables our transformation to make not just a specific method, such as PatchCore, unsupervised, but also any existing OCC anomaly detection method.

Our folding method, as shown in Table 2, is applicable across various methods. We employ a diverse selection of methods to demonstrate this, including memory bank-based approaches such as PatchCore and DinoAnomaly, as well as reconstruction-based methods and those that utilize student-teacher architectures, such as EfficientAD [3, 14, 33]. Our method renders all selected existing OCC image anomaly detectors highly tolerant to training anomaly corruptions.

Our proposed method links unsupervised anomaly detection as a complementary task to OCC anomaly detection, with improvements in OCC performance linked to improvements in the unsupervised task when folded, as seen in Table 2. Now, any future advancement in the highly active field of OCC anomaly detection will be a direct advancement in unsupervised anomaly detection.

We observe considerable improvements over the OCC baselines with 10% anomaly corruptions in the training data, as shown in Table 2. These differences are most pronounced in hard decision boundary methods, such as those that use patch-based nearest neighbor comparisons, and least pronounced in methods that have fuzzier boundaries, such as student-teacher and autoencoder methods [3, 33]. Notably, the improvement in the unsupervised case does not come at a significant cost in the OCC case, unlike that observed with the previous unsupervised methods. The reductions in OCC performance in our proposed folding method stem from removing some nominal data from the training set, thereby reducing the size of the final set. We expect that in real-world deployments of our method, the smaller filtered set can be compensated for by collecting more data without requiring manual inspection of the training data for anomalies.

## 4.3. Extension to Logical Anomalies

Notably, the method we selected to demonstrate the effectiveness of our folding procedure for student-teacher and autoencoder networks, EfficientAD, was designed for both logical and structural anomaly detection [3]. While structural anomalies may include foreign objects or dents, logical anomalies encompass issues such as excessive quantities of a nominal object or anomalous relationships between otherwise nominal objects. We assume no prior knowledge of the types of anomalies in our formulation of our folding method, only that the underlying OCC method performs well on the target anomalies. In Table 3 we show that our folding procedure can generalize to models designed for logical anomalies.

Corruptions	Metric	DinoAnomaly [14]		Reverse Distillation++ [37]		EfficientAD [3]	
		Baseline	Folded (1/4)	Baseline	Folded (1/4)	Baseline	Folded (1/4)
10%	I-AUROC	0.671	0.978	0.784	0.957	0.888	0.966
0%	I-AUROC	0.991	0.986	0.985	0.971	0.989	0.983

Nearest Neighbors, Patch Features      Reconstruction, Compression      Student Teacher, Autoencoder

Table 2. Performance of diverse OCC methods wrapped and unwrapped on corrupted and uncorrupted MvTecAD dataset in image AUROC [2]. Each method has its key architectural features listed below to show the diversity of methods.

Metric	0% Corruptions					10% Corruptions				
	SoftPatch [41]	FUN-AD [17]	Efficient-AD [3]	PUAD [35]		SoftPatch [41]	FUN-AD [17]	Efficient-AD [3]	PUAD [35]	
	Baseline	Baseline	Baseline	Baseline	Folded(1/4)	Baseline	Baseline	Baseline	Baseline	Folded(1/4)
I-AUROC	0.708	0.530	0.901	<b>0.923</b>	<u>0.911</u>	0.674	0.618	0.790	<u>0.811</u>	<b>0.849</b>
P-AUROC	0.704	0.693	<b>0.741</b>	<u>0.724</u>	0.704	0.670	<u>0.688</u>	0.670	0.668	<b>0.712</b>
AUPRO	0.501	0.356	<b>0.681</b>	<u>0.655</u>	0.635	0.479	0.392	<u>0.629</u>	0.622	<b>0.647</b>

Table 3. Performance of unsupervised and OCC supervised methods on corrupted and uncorrupted LOCO AD dataset [3].

detection. We expect this generalization to hold for any other type of anomaly formulation.

We choose to showcase our folding on PUAD, another OCC logical anomaly detection method, as it outperforms EfficientAD for logical anomaly detection [3, 35]. Folded PUAD in the 10% anomaly corruption task shows vastly greater performance than existing unsupervised anomaly detection baselines and considerable improvements over logical anomaly OCC baselines, see Table 3. This is because these unsupervised baselines were not designed to handle logical anomalies and therefore cannot generalize to them [3, 17, 41]. For contrasting reasons, existing logical OCC method baselines struggle with the training anomaly corruptions, degrading their test performance.

We observe that the gains in performance over the existing OCC logical anomaly detection baselines in the corrupted task are lower than in other tasks. This is because our folding procedure assumes the underlying methods are good OCC methods; however, as can be seen in Table 3, the logical anomaly detection task in the uncorrupted case is more difficult than the structural anomaly detection of MVTecAD and ViSA [2, 3, 49]. Despite this, as better OCC methods for logical anomaly detection are released, we expect those methods, when folded, to improve upon the unsupervised results shown today by adapting PUAD.

#### 4.4. Extension to Video Anomalies

For completeness in Table 4, we show results for folding DMAD, an OCC video anomaly detection method, on the Peds2 dataset [22, 24]. Again, our method makes no assumptions about the underlying anomaly types or data types, allowing it to be extended to video as described in Section 3.4. DMAD demonstrates strong anomaly tolerance

# of Corrupted Videos	0	6
Folded (3/2) DMAD	0.948	0.949
Baseline DMAD	0.944	0.928

Table 4. Performance of the DMAD video anomaly detector on the Peds2 dataset in frame-wise AUROC [22, 24]. The corrupted Peds2 dataset had 6 anomalous videos included in the training set. Folded DMAD used 2 folds and 3 votes [22, 24].

within its end-to-end fuzzy-decision-boundary deep learning architecture; however, this tolerance is further improved when operating on a corrupted dataset using our folding method. Our folding method even shows improvement in the OCC case, as we expect it to remove parts of videos that are poorly represented as nominal in the rest of the training data. In the case of corrupted training data, we further improve upon the OCC case by integrating additional nominal frames from the corrupted videos into the training data while pruning anomalies. This paper’s primary focus is not on video anomaly detection, because existing OCC video anomaly detectors generally rely on pre-trained human detectors or pose estimation as an initial task for human-focused anomaly detection [1, 28, 30, 40]. We consider this a separate problem from the purely unsupervised general anomaly detection on which this paper seeks to improve.

#### 4.5. Hyperparameters

We evaluate the selection of folding hyperparameters, the number of folds, and the number of votes on MvTecAD with 10% training anomaly corruptions in Table 5. We note a tradeoff in the number of folds used. If only two folds are

Votes ↓ Folds →	2	4	6	8
1	0.883	0.983	0.983	0.980
3	0.871	<b>0.984</b>	0.981	0.981
5	0.879	0.981	0.982	0.980

Table 5. Hyperparameter search for folding PatchCore on MvTecAD with 10% training corruptions using I-AUROC as the metric. [2, 33]

used, the anomalies are not sufficiently filtered, as they are too homogeneous with each other on the MvTecAD dataset. However, if too many folds are used, there is insufficient data to train the underlying PatchCore OCC effectively, resulting in poorer anomaly filtering as well. The proportion of the original dataset in each fold is  $1/n$ , where  $n$  is the number of folds, so for the toothbrush class of MvTecAD with 8 folds, only 7 images are used to train each instance of the underlying OCC to filter anomalies [2]. Regarding the number of votes, we note that generally using three votes rather than a single vote increases performance slightly, but significantly increases training time by a factor of almost three. Increasing the number of votes to 5 does not improve scores, despite the additional training time.

#### 4.6. Tolerance to Training Anomaly Rates

In Table 6, we evaluate our folding procedure on the MvTecAD dataset with varying anomaly training corruption proportions using PatchCore with 3 votes and 6 folds. Our method exhibits strong unsupervised performance, even in the worst-case scenario, where 40% of the training images contain anomalies. We see a steady decrease in performance as the proportion of anomalies in the training data increases. This is expected, as it begins to violate some of the assumptions underlying the folding procedure, namely that anomalies are infrequent in the dataset. This is exacerbated by the fact that all anomalies in the MvTecAD dataset used for this analysis are manually constructed to fit into a small set of anomaly categories; for example, the hazelnut class has only four anomaly categories [2]. This construction of anomalies to fit discrete categories breaks another assumption of our folding procedure, that the images being trained on are sampled independently of each other. Despite these challenges in the dataset, our folding procedure consistently maintains a high filter recall of over 92% of anomalies removed at all tested rates. This indicates that these assumptions are relatively soft requirements for our method to perform well, likely due to the high dimensionality of images.

#### 4.7. Training and Inference Speed

One significant benefit of our method is that it makes no modifications to the underlying OCC method at inference time. This makes our method as fast as the underlying OCC method used; for instance, we achieve the same sub-5ms

Corruption %	0.00	0.10	0.20	0.30	0.40
I-AUROC	0.992	0.981	0.972	0.949	0.938
P-AUROC	0.982	0.972	0.953	0.940	0.925
AUPRO	0.946	0.929	0.919	0.901	0.885
Filter Precision	∅	0.756	0.842	0.878	0.891
Filter Recall	∅	0.935	0.944	0.925	0.921

Table 6. Performance metrics under different anomaly corruption percentages on MvTecAD with Folded(3/6) PatchCore, 6 folds were used to increase tolerance to anomalies [2, 33].

inference latency reported by EfficientAD in our unsupervised results in Table 2 [3]. In fact, for methods which use a memory bank, such as PatchCore or DinoAnomaly, our folding procedure provides a slight increase in inference speed [14, 33]. This is because we remove anomalies and some poorly reinforced nominal data, making the memory bank at inference time smaller, reducing latency.

This parity with existing OCC methods at inference time does not hold for our method during training. The folding procedure requires retraining the model multiple times to predict anomalies in other folds. Generally, the training time is  $t(k \times n + 1)$  where  $t$  is the time to train the model once,  $k$  is the number of votes, and  $n$  is the number of folds. The additional 1 is the time to train the final model for inference on the filtered dataset, which takes  $t \times k \times n$  to be filtered. For our main configuration of 3 votes and 4 folds, this means we need to re-train the underlying OCC 13 times.

## 5. Conclusion

In this paper, we introduce a folding transformation that adapts arbitrary OCC anomaly detection methods to operate fully unsupervised, thereby retroactively removing the one-class assumptions of existing anomaly detection methods. Furthermore, as future improved OCC methods are developed, they will also be able to operate fully unsupervised using this procedure. Any improvement in the OCC state-of-the-art is likely to correlate with a direct improvement in the unsupervised state-of-the-art presented here. Finally, this transformation has also expanded the set of possible applications of fully unsupervised anomaly detection methods to the full scope of OCC methods, for instance, presenting the first fully unsupervised logical anomaly detection method.

### 5.1. Limitations

Our method requires significant increases in training time to supplement existing OCC methods with high tolerance to anomalies, on the order of 4-40 times longer across all of our testing configurations. This increase in training time is prohibitive for some domains, which may require online fine-tuning of the nominal model. Furthermore, since we make no changes to the underlying OCC methods, any lim-

itations of the underlying method also apply to the method after folding. For instance, some of the OCC methods used in this paper to achieve our state-of-the-art results rely on large pre-trained feature extractors, which limit their applicability to domains with image distributions similar to those of the pre-training tasks [14, 33].

## References

- [1] Sunghyun Ahn, Youngwan Jo, Kijung Lee, and Sanghyun Park. Videopatchcore: An effective method to memorize normality for video anomaly detection. In *Proceedings of the Asian Conference on Computer Vision*, pages 2179–2195, 2024. 7
- [2] Paul Bergmann, Michael Fauser, David Sattlegger, and Carsten Steger. Mvtac ad — a comprehensive real-world dataset for unsupervised anomaly detection. In *2019 IEEE/CVF Conference on Computer Vision and Pattern Recognition (CVPR)*, pages 9584–9592, 2019. 5, 6, 7, 8, 1, 3
- [3] Paul Bergmann, Kilian Batzner, Michael Fauser, David Sattlegger, and Carsten Steger. Beyond dents and scratches: Logical constraints in unsupervised anomaly detection and localization. *International Journal of Computer Vision*, 130(4):947–969, 2022. 1, 2, 5, 6, 7, 8, 3, 4
- [4] James C Bezdek, Sutharshan Rajasegarar, Masud Moshtaghi, Chris Leckie, Marimuthu Palaniswami, and Timothy C Havens. Anomaly detection in environmental monitoring networks [application notes]. *IEEE Computational Intelligence Magazine*, 6(2):52–58, 2011. 1, 2
- [5] Ankan Bhunia, Changjian Li, and Hakan Bilen. Looking 3d: Anomaly detection with 2d-3d alignment. In *Proceedings of the IEEE/CVF Conference on Computer Vision and Pattern Recognition*, pages 17263–17272, 2024. 1
- [6] Kim Bjerge, Quentin Geissmann, Jamie Alison, Hjalte MR Mann, Toke T Høye, Mads Dyrmann, and Henrik Karstoft. Hierarchical classification of insects with multitask learning and anomaly detection. *Ecological Informatics*, 77:102278, 2023. 2
- [7] Varun Chandola, Arindam Banerjee, and Vipin Kumar. Anomaly detection: A survey. *ACM computing surveys (CSUR)*, 41(3):1–58, 2009. 1, 2, 3
- [8] Zhen Cheng, Siwei Wang, Pei Zhang, Siqi Wang, Xinwang Liu, and En Zhu. Improved autoencoder for unsupervised anomaly detection. *International Journal of Intelligent Systems*, 36(12):7103–7125, 2021. 2
- [9] Yajie Cui, Zhaoxiang Liu, and Shigu Lian. A survey on unsupervised anomaly detection algorithms for industrial images. *IEEE Access*, 11:55297–55315, 2023. 2, 3
- [10] Thomas Defard, Aleksandr Setkov, Angelique Loesch, and Romaric Audigier. Padim: a patch distribution modeling framework for anomaly detection and localization. In *Pattern Recognition. January 10–15, 2021*, pages 475–489. Springer, 2021. 2
- [11] Tharindu Fernando, Harshala Gammulle, Simon Denman, Sridha Sridharan, and Clinton Fookes. Deep learning for medical anomaly detection—a survey. *ACM Computing Surveys (CSUR)*, 54(7):1–37, 2021. 1
- [12] Izhak Golan and Ran El-Yaniv. Deep anomaly detection using geometric transformations. *Advances in neural information processing systems*, 31, 2018. 2
- [13] Denis Gudovskiy, Shun Ishizaka, and Kazuki Kozuka. Cflow-ad: Real-time unsupervised anomaly detection with localization via conditional normalizing flows. In *Proceedings of the IEEE/CVF winter conference on applications of computer vision*, pages 98–107, 2022. 2

[14] Jia Guo, Shuai Lu, Weihang Zhang, Fang Chen, Huiqi Li, and Hongen Liao. Dinomaly: The less is more philosophy in multi-class unsupervised anomaly detection. In *Proceedings of the Computer Vision and Pattern Recognition Conference*, pages 20405–20415, 2025. 6, 7, 8, 9, 1, 3, 4

[15] Victoria Hodge and Jim Austin. A survey of outlier detection methodologies. *Artificial intelligence review*, 22(2):85–126, 2004. 3

[16] Hadi Hojjati, Thi Kieu Khanh Ho, and Narges Armanfard. Self-supervised anomaly detection in computer vision and beyond: A survey and outlook. *Neural Networks*, 172:106106, 2024. 2

[17] Jiin Im, Yongho Son, and Je Hyeong Hong. Fun-ad: Fully unsupervised learning for anomaly detection with noisy training data. In *2025 IEEE/CVF Winter Conference on Applications of Computer Vision (WACV)*, pages 9447–9456. IEEE, 2025. 2, 3, 6, 7

[18] Nathalie Japkowicz, Catherine Myers, Mark Gluck, et al. A novelty detection approach to classification. In *IJCAI*, pages 518–523. Citeseer, 1995. 2

[19] Ki Hyun Kim, Sangwoo Shim, Yongsub Lim, Jongseob Jeon, Jeongwoo Choi, Byungchan Kim, and Andre S Yoon. Rapp: Novelty detection with reconstruction along projection pathway. In *International Conference on Learning Representations*, 2020. 2

[20] Ruiyang Liu, Weiming Liu, Zhongxing Zheng, Liang Wang, Liang Mao, Qisheng Qiu, and Guangzheng Ling. Anomaly-gan: A data augmentation method for train surface anomaly detection. *Expert Systems with Applications*, 228:120284, 2023. 2

[21] Tianmou Liu, Han Yu, and Rachael Hageman Blair. Stability estimation for unsupervised clustering: A review. *WIREs Computational Statistics*, 14(6):e1575, 2022. 2

[22] Wenrui Liu, Hong Chang, Bingpeng Ma, Shiguang Shan, and Xilin Chen. Diversity-measurable anomaly detection. In *Proceedings of the IEEE/CVF Conference on Computer Vision and Pattern Recognition (CVPR)*, pages 12147–12156, 2023. 6, 7, 4

[23] Zijun Long, Lipeng Zhuang, George Killick, Richard McCreadie, Gerardo Aragon-Camarasa, and Paul Henderson. Understanding and mitigating human-labelling errors in supervised contrastive learning. In *European Conference on Computer Vision*, pages 435–454. Springer, 2024. 2

[24] Vijay Mahadevan, Weixin Li, Viral Bhalodia, and Nuno Vasconcelos. Anomaly detection in crowded scenes. In *2010 IEEE Computer Society Conference on Computer Vision and Pattern Recognition*, pages 1975–1981, 2010. 7

[25] Fabrizio Mastro and Annamaria Porreca. Environmental loss assessment via functional outlier detection of transformed biodiversity profiles. *Journal of Agricultural, Biological and Environmental Statistics*, pages 1–22, 2024. 2

[26] Declan McIntosh and Alexandra Branzan Albu. Inter-realization channels: Unsupervised anomaly detection beyond one-class classification. In *Proceedings of the IEEE/CVF International Conference on Computer Vision*, pages 6285–6295, 2023. 2, 3, 4, 5, 6

[27] Declan McIntosh and Alexandra Branzan Albu. Unsupervised, online and on-the-fly anomaly detection for non-stationary image distributions. In *European Conference on Computer Vision*, pages 428–445. Springer, 2024. 2, 3

[28] Pratik K Mishra, Alex Mihailidis, and Shehroz S Khan. Skeletal video anomaly detection using deep learning: Survey, challenges, and future directions. *IEEE Transactions on Emerging Topics in Computational Intelligence*, 8(2):1073–1085, 2024. 7

[29] Ali Bou Nassif, Manar Abu Talib, Qassim Nasir, and Fatima Mohamad Dakalbab. Machine learning for anomaly detection: A systematic review. *Ieee Access*, 9:78658–78700, 2021. 1

[30] Bharathkumar Ramachandra, Michael J Jones, and Ranga Raju Vatsavai. A survey of single-scene video anomaly detection. *IEEE transactions on pattern analysis and machine intelligence*, 44(5):2293–2312, 2020. 7

[31] Douglas A. Reynolds. Gaussian mixture models. In *Encyclopedia of Biometrics*, 2018. 5

[32] Oliver Rippel, Patrick Mertens, Eike König, and Dorit Merhof. Gaussian anomaly detection by modeling the distribution of normal data in pretrained deep features. *IEEE Transactions on Instrumentation and Measurement*, 70:1–13, 2021. 2

[33] Karsten Roth, Latha Pemula, Joaquin Zepeda, Bernhard Schölkopf, Thomas Brox, and Peter Gehler. Towards total recall in industrial anomaly detection. In *Proceedings of the IEEE/CVF Conference on Computer Vision and Pattern Recognition*, pages 14318–14328, 2022. 2, 5, 6, 8, 9, 1, 3, 4

[34] Marco Rudolph, Tom Wehrbein, Bodo Rosenhahn, and Bastian Wandt. Asymmetric student-teacher networks for industrial anomaly detection. In *Proceedings of the IEEE/CVF winter conference on applications of computer vision*, pages 2592–2602, 2023. 2

[35] Shota Sugawara and Ryuji Imamura. Puad: Frustratingly simple method for robust anomaly detection, 2024. 7

[36] Peng Tang, Xiaoxiao Yan, Xiaobin Hu, Kai Wu, Tobias Lasser, and Kuangyu Shi. Anomaly detection in medical images using encoder-attention-2decoders reconstruction. *IEEE Transactions on Medical Imaging*, 2025. 2

[37] Tran Dinh Tien, Anh Tuan Nguyen, Nguyen Hoang Tran, Ta Duc Huy, Soan T.M. Duong, Chanh D. Tr. Nguyen, and Steven Q. H. Truong. Revisiting reverse distillation for anomaly detection. In *Proceedings of the IEEE/CVF Conference on Computer Vision and Pattern Recognition (CVPR)*, pages 24511–24520, 2023. 7, 1, 3, 4

[38] Tomas Vojir, Tomáš Šipka, Rahaf Aljundi, Nikolay Chumerin, Daniel Olmeda Reino, and Jiri Matas. Road anomaly detection by partial image reconstruction with segmentation coupling. In *Proceedings of the IEEE/CVF International Conference on Computer Vision*, pages 15651–15660, 2021. 2

[39] Chengjie Wang, Wenbing Zhu, Bin-Bin Gao, Zhenye Gan, Jiangning Zhang, Zhihao Gu, Shuguang Qian, Mingang Chen, and Lizhuang Ma. Real-iad: A real-world multi-view dataset for benchmarking versatile industrial anomaly detection. In *Proceedings of the IEEE/CVF Conference on Com-*

puter Vision and Pattern Recognition, pages 22883–22892, 2024. [1](#)

- [40] Guodong Wang, Yunhong Wang, Jie Qin, Dongming Zhang, Xiuguo Bao, and Di Huang. Video anomaly detection by solving decoupled spatio-temporal jigsaw puzzles. In *European Conference on Computer Vision*, pages 494–511. Springer, 2022. [7](#)
- [41] Jiang Xi, Jianlin Liu, Jinbao Wang, Qiang Nie, WU Kai, Yong Liu, Chengjie Wang, and Feng Zheng. Softpatch: Unsupervised anomaly detection with noisy data, 2024. [1](#), [2](#), [3](#), [4](#), [5](#), [6](#), [7](#)
- [42] Xuan Xia, Xizhou Pan, Nan Li, Xing He, Lin Ma, Xiaoguang Zhang, and Ning Ding. Gan-based anomaly detection: A review. *Neurocomputing*, 493:497–535, 2022. [2](#)
- [43] Pei Xiang, Shahzad Ali, Soon Ki Jung, and Huixin Zhou. Hyperspectral anomaly detection with guided autoencoder. *IEEE Transactions on Geoscience and Remote Sensing*, 60: 1–18, 2022. [2](#)
- [44] Tiange Xiang, Yixiao Zhang, Yongyi Lu, Alan L Yuille, Chaoyi Zhang, Weidong Cai, and Zongwei Zhou. Squid: Deep feature in-painting for unsupervised anomaly detection. In *Proceedings of the IEEE/CVF Conference on Computer Vision and Pattern Recognition*, pages 23890–23901, 2023. [2](#)
- [45] Lei Xie, Tao Guo, Jiliang Chang, Chengpeng Wan, Xinyuan Hu, Yang Yang, and Changkui Ou. A novel model for ship trajectory anomaly detection based on gaussian mixture variational autoencoder. *IEEE Transactions on Vehicular Technology*, 72(11):13826–13835, 2023. [2](#)
- [46] Jihun Yi and Sungroh Yoon. Patch svdd: Patch-level svdd for anomaly detection and segmentation. In *Proceedings of the Asian Conference on Computer Vision*, 2020. [2](#)
- [47] Vitjan Zavrtanik, Matej Kristan, and Danijel Skočaj. Reconstruction by inpainting for visual anomaly detection. *Pattern Recognition*, 112:107706, 2021. [2](#)
- [48] Xuan Zhang, Shiyu Li, Xi Li, Ping Huang, Jiulong Shan, and Ting Chen. Destseg: Segmentation guided denoising student-teacher for anomaly detection. In *Proceedings of the IEEE/CVF conference on computer vision and pattern recognition*, pages 3914–3923, 2023. [2](#)
- [49] Yang Zou, Jongheon Jeong, Latha Pemula, Dongqing Zhang, and Onkar Dabeer. Spot-the-difference self-supervised pre-training for anomaly detection and segmentation. In *Computer Vision – ECCV 2022*, pages 392–408, Cham, 2022. Springer Nature Switzerland. [6](#), [7](#), [2](#)
- [50] Yang Zou, Jongheon Jeong, Latha Pemula, Dongqing Zhang, and Onkar Dabeer. Spot-the-difference self-supervised pre-training for anomaly detection and segmentation. In *Computer Vision–ECCV 2022: 17th European Conference, Tel Aviv, Israel, October 23–27, 2022, Proceedings, Part XXX*, pages 392–408. Springer, 2022. [2](#)

# Universal Transformation of One-Class Classifiers for Unsupervised Anomaly Detection

## Supplementary Material

### 6. Qualitative Comparisons

We show some additional qualitative comparisons between our method and other baselines. Images and plots are best viewed zoomed in. Images were selected to maximize the difference in anomaly predictions, thereby making the selected images more informative. See Figures 4 & 5.

As expected from the quantitative results and the similar underlying architectures, both folded PatchCore and Soft-Patch perform very similarly despite filtering anomalies at very different stages, image-wise against patch-wise. Both FUN-AD and InReaCh show worse qualitative performance, with occasional false negatives and false positives in the selection, though selecting for differences in prediction overstates the relative difference in actual performance.

In the first row of the logical case, showing breakfast boxes, in Figure 5, it can be seen that the unsupervised methods not tuned for logical anomaly detection greatly overestimate the anomalous region. In contrast, the OCC logical methods greatly underestimate it. In the second row of splicing connectors, you can see that all methods detect this structural anomaly, but the patch-based methods are generally more confident in their detection. In the bottom row of the figure showing results on a juice bottle missing its juice, this image was used during training, and both the unsupervised non-logical methods find the anomaly well, with some over-prediction. Still, the OCC logical methods miss this anomaly entirely, whereas Folded PUAD shows some detection of it.

### 7. Ensemble Folding

Since each fold of our method trains an OCC method independently of the others, all the trained OCC methods need not be the same. We considered that an ensemble of models trained on each fold might perform better, similar to boosting. We found in testing that an ensemble of PatchCore [33], DinoAnomaly [14], Reverse Distillation++ [37], and EfficientAD [3], then training a final PatchCore model on the filtered dataset, performed worse than using PatchCore on its own, see Table 7. In the future, though, it may be best to use one slower but better anomaly detector to filter the dataset, then train a final, worse anomaly detector with faster inference for deployment.

Metric	Ensemble (1/4)	PatchCore (1/4)
I-AUROC	0.972	<b>0.983</b>
P-AUROC	0.957	<b>0.974</b>
AUPRO	0.917	<b>0.935</b>

Table 7. Performance of Ensemble(1/4) consisting of PatchCore [33], DinoAnomaly [14], Reverse Distillation++ [37], and EfficientAD [3] compared against folded PatchCore(1/4) on MvTecAD [2] with 10% training corruptions.

### 8. Additional Fold Prediction Distributions and Gaussian Fits

In Figure 6, it can be observed that the large majority of anomalies present for that fold are correctly predicted as anomalies by the filter. Notably, the normalized confidence threshold differs significantly across classes, and even by manual inspection, it is clear that a fixed threshold would not perform well. This motivated the use of a Mixture of Gaussians to set the anomaly filter cutoff threshold dynamically. It is also beneficial that dynamically determining this filter threshold removes a hyperparameter from the method.

For some classes, such as the Pill class, it can be seen that some anomalies have very low predictions, well into the distribution of the nominal sample’s predictions. These samples are not filtered, as the OCC method does not pick up on the anomalies in those images. Since the model used to predict on these images was trained on a separate, independent set, even if those anomalies were not in the training data, the underlying OCC method is likely to miss them. These issues can likely only be addressed by an even better future OCC method beyond the scope of this work.

### 9. Folding Already Unsupervised Methods

Another question we tested but determined did not work well was whether folding existing unsupervised anomaly detection methods would improve their performance in the unsupervised case. To test this in Table 8, we tested each of the existing unsupervised baselines folded (1/4) and unfolded on the MvTecAD dataset with 10% training corruptions. We found little to no improvement for both InReaCh and SoftPatch, as they both are already good anomaly filters, and adding another filter on top only reduced the apparent dataset size for these methods. FUN-AD had a much worse response to the apparent dataset reduction from the folding method, performing much worse when folded, indicating that it is less sample efficient than the other methods

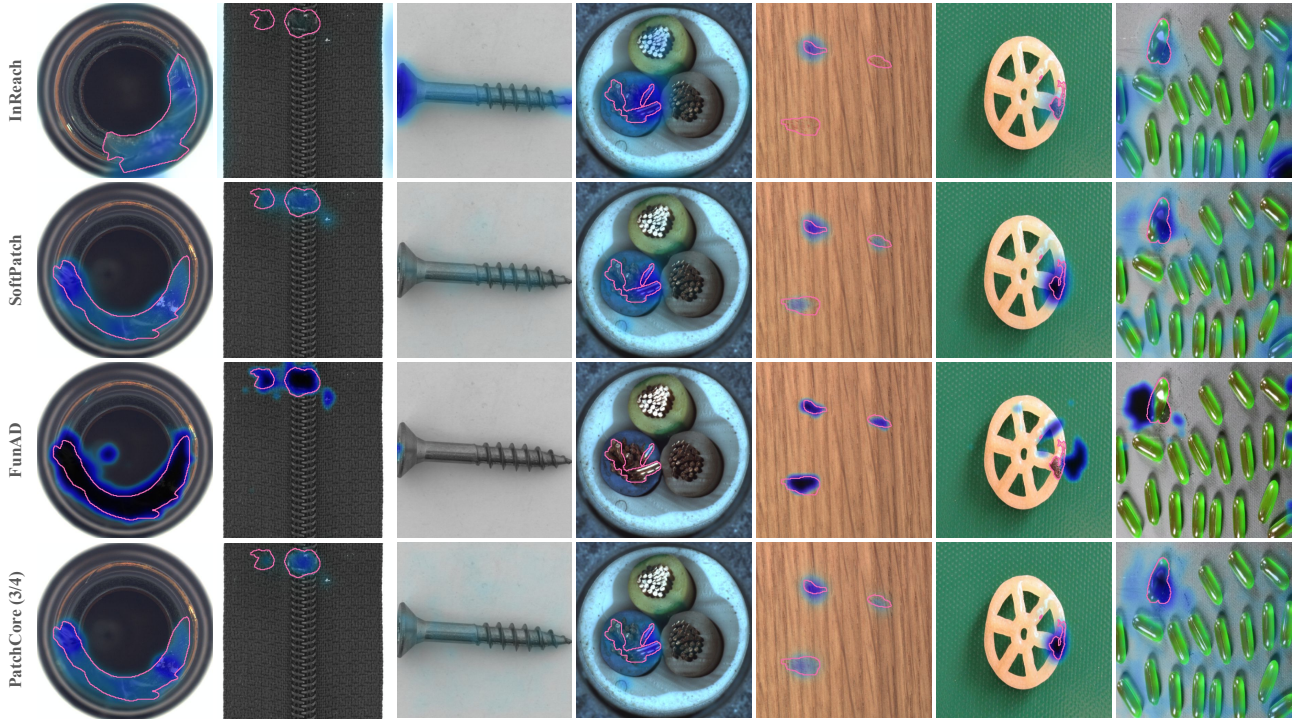


Figure 4. Qualitative results of unsupervised methods on MvTecAD and VisA[49].

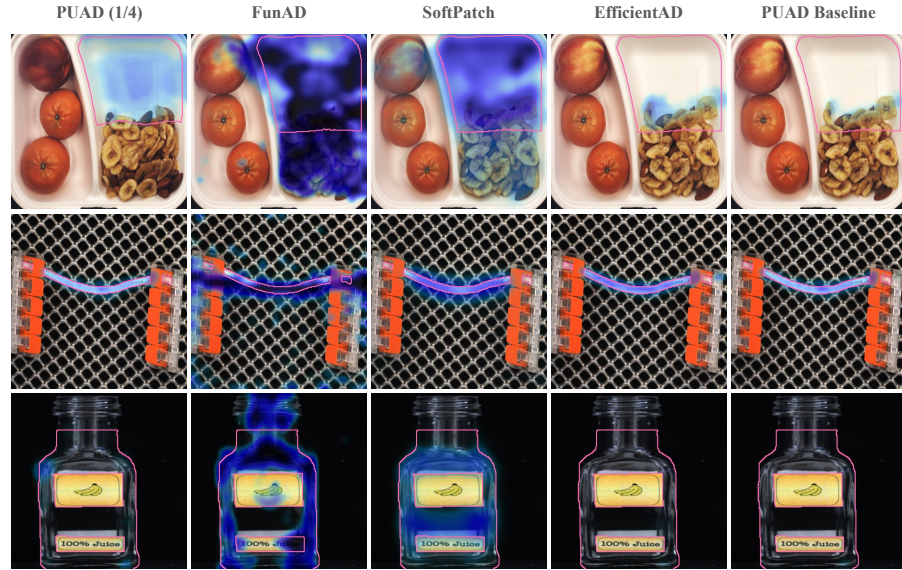


Figure 5. Qualitative results of unsupervised baselines (SoftPatch, FUN-AD), and OCC logical baselines (PUAD, EfficientAD) on Loco AD dataset [3].

for building its nominal model.

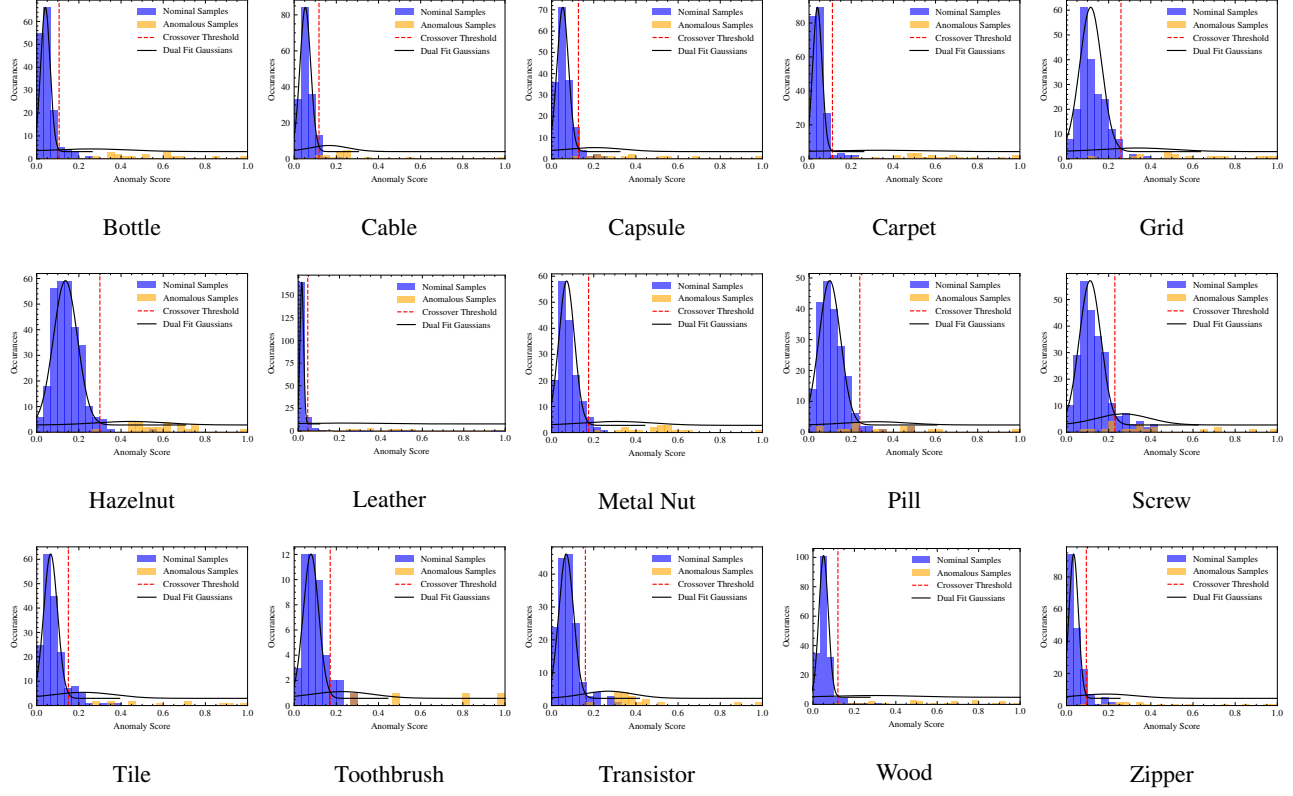


Figure 6. Example Fit Gaussian distributions on data from the first fold and the first vote of all classes in the MvTecAD dataset [2] with PatchCore(3/4) [33]. Determined thresholds for the anomaly filter for that fold are shown in a red dotted line. Best viewed zoomed in digitally.

Metric	InReCh	InReach(1/4)	SoftPatch	SoftPatch(1/4)	FUN-AD	FUN-AD(1/4)
I-AUROC	0.855	0.862	0.984	0.976	0.965	0.837
P-AUROC	0.935	0.944	0.960	0.979	0.975	0.934
AUPRO	0.805	0.804	0.903	0.925	0.888	0.730

Table 8. Performance of Ensemble(1/4) consisting of PatchCore [33], DinoAnomaly [14], Reverse Distillation++ [37], and EfficientAD [3] compared against folded PatchCore(1/4) on MvTecAD [2] with 10% training corruptions.

## 10. Implementation Details of Folded and Baseline Methods

For all presented results, there are no modifications of the underlying methods between when they are used folded and unfolded.

### 10.1. InReCh [26]

We use the official code for InReCh without modification.

### 10.2. SoftPatch [41]

We use the official code for SoftPatch without modification.

### 10.3. FUN-AD [17]

We use the official code for FUN-AD with modifications. Firstly, we removed the original implementation's use of

the testing set as a validation set for selecting the best-performing checkpoint for reporting results. Since we are using this method as a baseline for existing unsupervised methods, test set labels cannot be used during training. We instead train for a number of epochs that gives approximately 40000 training steps. We determined this length based on the number of steps used to reach convergence on all classes of the MvTec AD dataset. FUN-AD also uses a synthetic dataset of corrupted nominal images from the MvTec AD dataset to report its performance on MvTec AD. Since no script was provided to generate these images for other datasets we use, such as VisA, we choose to exclude these additional training images. This leads to poor performance of FUN-AD in the 0% corruption cases, as the method assumes anomalies exist in the training data.

#### 10.4. PatchCore [33]

We use the official code for PatchCore without modification. We choose to use the PatchCore ensemble variation for it's higher performance.

#### 10.5. DinoAnomaly [14]

We use the official code for DinoAnomaly without modification.

#### 10.6. Reverse Distillation++ [37]

We use the official code for Reverse Distillation++ with modifications to the training length. The original method uses a custom number of training epochs for each MvTec AD class. We fix the maximum training epochs at 300, with early stopping on a plateau of loss for 15 epochs. We find minimal change in performance with this change, but it removes the reliance on a manually set training length for each dataset.

#### 10.7. EfficientAD [3]

We use the unofficial code released on GitHub (nelson1425/EfficientAD), which closely replicates the results of the original paper. No modifications to the code's core functionality were made to adapt it to the folding wrapper.

#### 10.8. DMAD [22]

We use the official code, which shows very close replication to the original paper. Modifications were made to remove the code components that use test set data to select the best checkpoint during training, and instead use a fixed training duration of 10 epochs. Removing access to testing data for training broke replication of the original paper's results for image anomaly detection, so it was excluded from our comparisons.